Wind and Structures, *Vol. 30, No. 2 (2020) 119-131*
DOI: https://doi.org/10.12989/was.2020.30.2.119

Experimental studies on the aerodynamic performance of two box girders with side openings

Jiaqi Wang*[1], Tomomi Yagi[1a], Jun Ushioda[1b], Kyohei Noguchi[1c], Naoki Nagamoto[2d] and Hiroyuki Uchibori[2e]

[1]*Dept. of Civil and Earth Resources Engineering, Kyoto Univ., Kyotodaigaku-Katsura, Nishikyo-ku, Kyoto 615-8540, Japan*
[2]*Structural Engineering Service Dept., Sumitomo Mitsui Construction co., ltd., Tsukuda, Chuou-ku, Tokyo 104-0051, Japan*

(Received September 10, 2018, Revised June 1, 2019, Accepted November 26, 2019)

Abstract. A butterfly web girder is a box-shaped girder with discretely distributed side openings along the spanwise direction. Until now, there have been few studies related to the aerodynamic performance of the butterfly web bridge. The objective of the current study was to clarify the effects of the side openings on the aerodynamic performance of the girder. Two butterfly web girders with side ratios B/D = 3.24 and 5, where B is the girder width and D is the depth, were examined through a series of wind tunnel tests. A comparison of the results for butterfly web girders and conventional box girders of the same shape confirmed that the side openings stabilized the vortex-induced vibration and galloping when B/D = 3.24, whereas the vortex-induced vibration and torsional flutter were stabilized when B/D = 5. The change in the flow field due to the side openings contributed to the stabilization against the vibration. These findings not only confirmed the good aerodynamic performance of the butterfly web bridge but also provided a new method to stabilize the box girder against aerodynamic instabilities via discretely distributed side openings.

Keywords: butterfly web bridge; galloping; torsional flutter; vortex-induced vibration; Kármán vortex

1. Introduction

A bridge always requires light and strong girders with good aerodynamic performance. A new type of girder, the butterfly web girder, was recently introduced. This girder can be viewed as a box girder with discretely distributed side openings (Fig. 1) and has advantages in terms of structure, construction, and maintenance (Kasuga 2017). The side openings reduce the weight of a butterfly web girder bridge, making it comparable to a corrugated-steel web girder bridge. However, in pursuing lightness and strength for the girder, the importance of the aerodynamic performance cannot be neglected (Billah and Scanlan 1991). Therefore, the concern is whether the side openings can stabilize the box girder against aerodynamic instabilities.

A butterfly web bridge with a side ratio of B/D = 5, where B is the girder width and D is the girder depth, was confirmed to be stabilized against vortex-induced vibration and torsional flutter by the discretely distributed side openings by a previous study (Kasuga 2015). However, that research was limited to a butterfly web girder with a side ratio of B/D = 5. Because the aerodynamic performance of a bluff body is generally characterized by the side ratio, the effects of side openings on the aerodynamic performance of box girders with different side ratios was investigated in the current study by examining two butterfly web girders with B/D = 3.24 and 5. The former was designed for the main girder of a 365-m extradosed bridge with a main span of 180 m, and the latter was designed for the main girder of a 500-m five-span extradosed bridge. Two conventional box girders of the same shape as the butterfly web girders were also examined, to compare the effects of side openings on aerodynamic performance.

Fig. 1 Butterfly web girder (Takubogawa Bridge)

*Corresponding author, Ph.D. Student
E-mail: wang.jiaqi.4n@gmail.com
[a] Professor, Ph.D.
E-mail: yagi.tomomi.7a@kyoto-u.ac.jp
[b] Former Master Student
[c] Assistant Professor, Ph.D.
E-mail: noguchi.kyohei.7z@kyoto-u.ac.jp
[d] Engineer, Ph.D.
E-mail: nagamoton@smcon.co.jp
[e] Engineer
E-mail: huchibori@smcon.co.jp

http://www.techno-press.com/journals/was&subpage=7

ISSN: 1226-6116 (Print), 1598-6225 (Online)

As a bluff body, the aerodynamic performance of a conventional box girder can generally be characterized as that of a rectangular cylinder of the same *B/D* ratio. Therefore, according to previous studies (Okajima *et al*. 1990, Matsumoto *et al*. 2008a), a conventional box girder of *B/D* = 3.24 may show vortex-induced vibration, galloping instability at a certain angle of attack, and torsional flutter, whereas at *B/D* = 5, the conventional box girder may show vortex-induced vibration and torsional flutter. However, owing to the discretely distributed side openings, it is difficult to make assumptions about the aerodynamic performance of a butterfly web girder.

Vortex-induced vibration can be roughly divided into two types: the Kármán-vortex and motion-induced types (Komatsu and Kobayashi 1980, Shiraishi and Matsumoto 1983, Nakamura and Nakashima 1986, Naudascher and Wang 1993, Wu and Kareem 2012, Nguyen *et al*. 2018). The Kármán-vortex vibration usually occurs at the reduced wind velocity of $1/St$. The onset of reduced wind velocity in motion-induced vortex vibration can be explained by the following equations (Matsumoto *et al*. 2008a)

Vertical motion

$$U_{cr} = \frac{1}{N}\frac{1}{0.6}\frac{B}{D} = \frac{1}{N}1.67\frac{B}{D} \quad (1)$$

Torsion motion:

$$U_{cr} = \frac{2}{2N-1}\frac{1}{0.6}\frac{B}{D} = \frac{2}{2N-1}1.67\frac{B}{D} \quad (2)$$

where N = 1, 2, … The two conventional box girders used in this study were expected to exhibit motion-induced vortex vibration rather than Kármán vortex vibration (Shiraishi and Matsumoto 1983, Nguyen *et al*. 2018). Due to shear layer instability, motion-induced vortices generate motion-induced vortex vibration (Shiraishi and Matsumoto 1983, Nakamura and Nakashima 1986, Naudascher and Wang 1993, Wu and Kareem 2012, Nguyen *et al*. 2018). However, discretely distributed side openings cause the flow to get through the girder. The outflow from the side openings into the wake may affect the formation of these vortices at the trailing edge, potentially affecting the coalescence of vortices from the leading and trailing edges (Deniz and Staubli 1997, Hourigan *et al*. 2001, Mills *et al*. 2003, Kumar *et al*. 2009). Therefore, the effects of side openings on motion-induced vortex vibration must be investigated.

Galloping is a type of divergent vertical vibration that occurs at high wind velocities, usually in rectangular cylinder-like bluff bodies with small *B/D* ratios (Nakamura *et al*. 1991a and 1994, Parkinson and Smith 1964, Naudascher *et al*. 1981, Hu *et al*. 2016). Galloping occurs because in a rectangular cylinder-like bluff body with a non-reattachment flow pattern, a downward motion of the body at high wind velocity can induce a downward pressure force (Parkinson and Sullivan 1979, Mizota and Okajima 1981, Nakamura *et al*. 1991, 1994, Hu *et al*. 2016). The Kármán vortex plays an important role in mitigating galloping instability (Matsumoto *et al*. 2008b, Yagi *et al*. 2013). Nakato (2016) confirmed that Kármán vortex shedding can be suppressed with side openings by controlling the fluctuating lift coefficient of a square cylinder. Because the outflow from the side openings of a butterfly web girder interferes with vortex shedding during vibration, it is important to determine whether the side openings can simultaneously suppress Kármán vortex shedding and mitigate galloping.

Torsional flutter is a divergent type of torsional vibration that is closely related to vortex convection along the surface and the locally separated flow near the leading edge (Matsumoto *et al*. 1997, Andrianne and Dimitriadis 2013). Because side openings may have effects on the unsteady flow around the body, their effects on torsional flutter should also be investigated.

Furthermore, the flow field around a rectangular cylinder with discretely distributed side openings has three-dimensional properties owing to section differences along the span-wise direction (Nakato 2016). These three-dimensional characteristics of the flow field may reduce the aerodynamic forces' span-wise correlation, which is sensitive to the vibration pattern and its amplitude (Li *et al*. 2016). Therefore, the three-dimensional flow may contribute to the effects of side openings on aerodynamic performance.

The purpose of the present study was to investigate the effects of side openings on aerodynamic performance. A series of wind tunnel tests was conducted on two butterfly web girders and two conventional box girders of the same shape. The wind tunnel tests consisted of aerodynamic force, free vibration, and forced vibration tests. To determine the effects of side openings, the aerodynamic responses and aerodynamic damping of the butterfly web and conventional box girders were monitored. To facilitate observation of the effects of side openings on the aerodynamic response, low values were assigned to the mass and damping of the free vibration system. The wind velocity distribution in the wake of the girder was also examined to investigate potential reasons for the effects of side openings on Kármán vortex shedding and galloping. These findings confirm the good aerodynamic performance of the butterfly web girder and provide a new method to control aerodynamic instability.

2. Wind tunnel test details

For the *B/D* = 3.24 model, the authors conducted wind-velocity measurements in the wake of the girder and tests of aerodynamic force, spring-supported free vibration (vertical one degree of freedom (1DOF)), and forced vibration (vertical 1DOF, torsional 1DOF). For the *B/D* = 5 model, the authors conducted free vibration tests (vertical 1DOF, torsional 1DOF) and forced vibration tests (torsional 1DOF). Wind tunnel measurements were conducted for both models in a room-circuit Eiffel wind tunnel at Kyoto University. The wind tunnel had a working section 1.8 m tall and 1.0 m wide. The maximum wind velocity was 30 m/s and the turbulence intensity of the smooth flow in the working section was 0.3%.

2.1 Model details

Two butterfly web girder sectional models were adopted in this research, one with a 1:80 geometrical scale and *B/D*

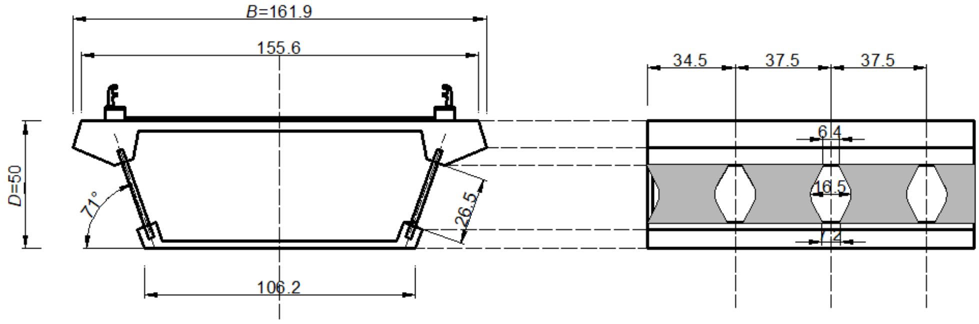

Fig. 2 Section of the B/D = 3.24 side ratio model and side opening detail (unit: mm)

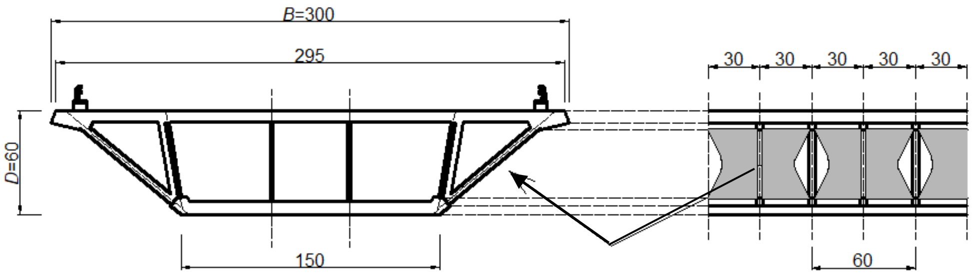

Fig. 3 Section of the B/D = 5 model and side opening detail (unit: mm)

ratio of 3.24, and the other with a 1:100 geometrical scale and a B/D ratio of 5. The cross sections and side openings of each model are shown in Figs. 2 and 3, respectively. The width (B) and depth (D) of the model with a B/D ratio of 3.24 were 161.9 mm and 50 mm, respectively, and those of the B/D = 5 model were 300 mm and 60 mm, respectively. The opening area ratio is defined by the ratio between the opening area and the total area of the front/rear surface. The opening area ratio is 15.5% for the B/D = 3.24 model and 16.7% for the B/D = 5 model. For the convenience of discussion, a butterfly web girder is defined as an open girder, and a conventional box girder of the same shape as the butterfly web girder is defined as a closed girder. A conventional box girder can be realized by covering the side openings of a butterfly web girder with an acrylic plate. To understand this better, open girders with B/D = 3.24 and 5 are shown in Figs. 4(a) and (b), respectively, and closed girders with B/D = 3.24 and 5 are shown in Figs. 4(c) and (d), respectively. Additionally, as shown in Fig. 5, at a certain angle of attack (α) due to the mean wind, the model has an equivalent length (B') and depth (D').

2.2 Aerodynamic force tests

In the aerodynamic force experiment, the model was rigidly connected to load cells and three aerodynamic forces were then measured. The data was recorded in a sampling frequency of 1000Hz. The angle of attack (α) ranged from −10 to 10° in 1° intervals and was defined as nose-up positive.

The three aerodynamic force coefficients (lift: C_{Fy}, drag: C_{Fx}, and pitching moment: C_M), Strouhal number St, and fluctuating lift force coefficient C_{Fy}' are defined on the structural axis as follows

$$C_{Fy} = \frac{F_y}{\frac{1}{2}\rho U^2 Bl} \tag{3}$$

$$C_{Fx} = \frac{F_x}{\frac{1}{2}\rho U^2 Dl} \tag{4}$$

$$C_M = \frac{F_M}{\frac{1}{2}\rho U^2 B^2 l} \tag{5}$$

$$S_t = \frac{f_{st} D}{U} \tag{6}$$

$$C'_{Fy} = \frac{F_y{}'(t)_{std}}{\frac{1}{2}\rho U^2 Bl} \tag{7}$$

where F_y, F_x, and F_M are the mean values of lift force (N), drag force (N), and pitching moment (N·m) defined on the structural axis (Fig. 6); l is the span length, ρ is the air density (kg/m^3), U is the approaching wind velocity (m/s), f_{st} is the dominant frequency (Hz) of the Kármán-vortex shedding, F_y(t) is the fluctuating lift force time series, F_y'(t) is the lift force component fluctuating in the frequency of f_{st}, F_y'$(t)_{std}$ is the standard deviation of F_y'(t). f_{st} was identified from the fluctuating lift force F_y(t), and F_y'(t) was calculated by applying a bandpass filter with a center frequency of f_{st} to the fluctuating lift force F_y(t).

Based on the quasi-steady theory, galloping occurs when the lift slope ($dC_{Fy}/d\alpha$) is negative, that is, the well-known Den Hartog criterion (Den Hartog 1985). Furthermore, the Kármán vortex shedding intensity, which indicates the strength of Kármán vortex shedding, is defined by the fluctuating lift force coefficients C_{Fy}'. The drag coefficient C_{Fx} is sensitive to the Kármán vortex shedding intensity. Strong vortex shedding is accompanied by strong roll-up of the separating shear layers at the near wake and negative base pressure of a large absolute value, which leads to a large C_{Fx} (Bearman and Trueman 1972, Matsumoto *et al.* 2006, Dong *et al.* 2017).

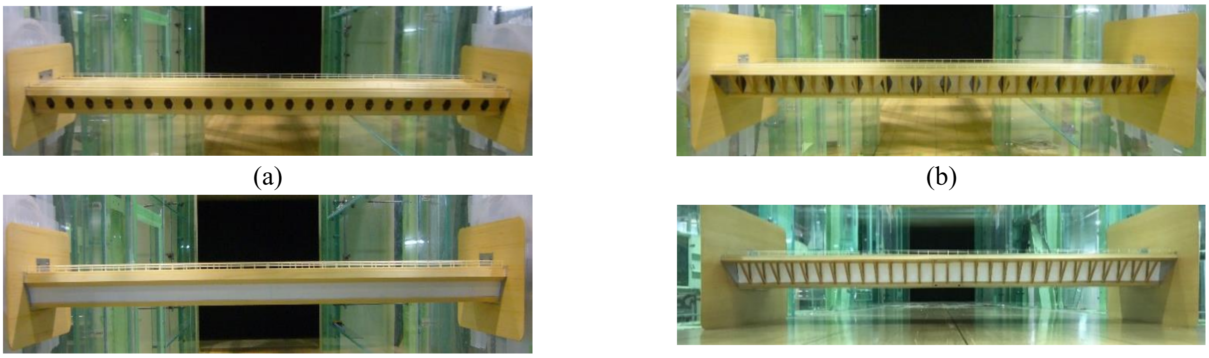

(a) (b) (c) (d)

Fig. 4 Models used in the experiment: (a) open girder (*B*/*D* = 3.24), (b) open girder (*B*/*D* = 5), (c) closed girder (*B*/*D* = 3.24, side openings covered), (d) closed girder (*B*/*D* = 5, side openings covered)

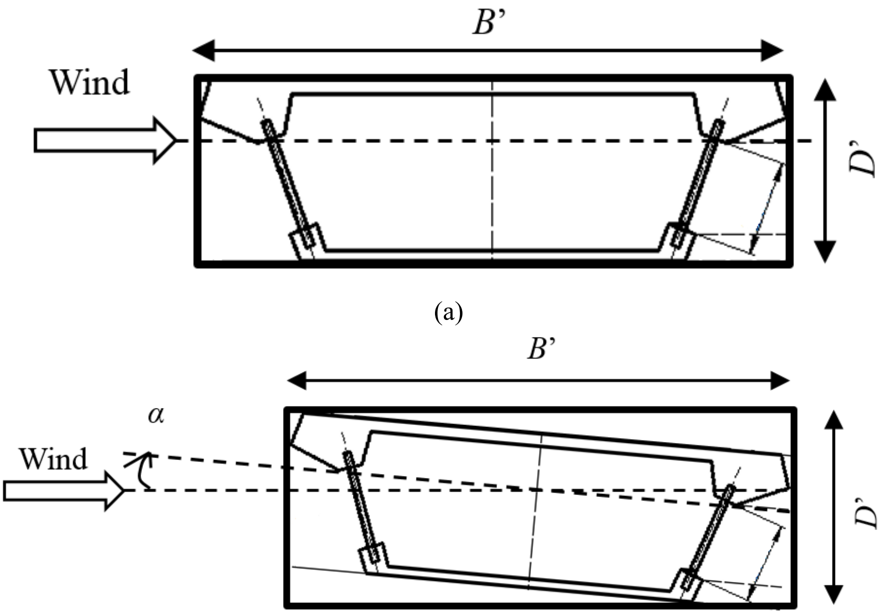

(b)

Fig. 5 Equivalent size of the model. (a) shows the case at α = 0°, (b) shows the case at α = +3°, α is the angle of attack due to mean wind

2.3 Free vibration tests

Both the *B/D* = 5 and *B/D* = 3.24 models must show the torsional flutter. The *B/D* = 3.24 model may show galloping at a certain angle of attack. To avoid the interference between the vertical and torsional vibrations, vertical/torsional 1DOF free vibration tests were applied in this research to evaluate the effects of side openings on aerodynamic performance, that is, vortex-induced vibration, galloping, and torsional flutter. A vertical 1DOF free vibration test was conducted for the *B/D* = 3.24 model, and vertical 1DOF and torsional 1DOF free vibration tests were conducted for the *B/D* = 5 model. Supported by eight coil springs, the displacement of the girder in smooth flow was measured at α = 0°, −3°, and +3° using laser gages. Low values were assigned to the mass and damping of the system to facilitate observation of the effects of the side openings on the aerodynamic properties (Tables 1–3).

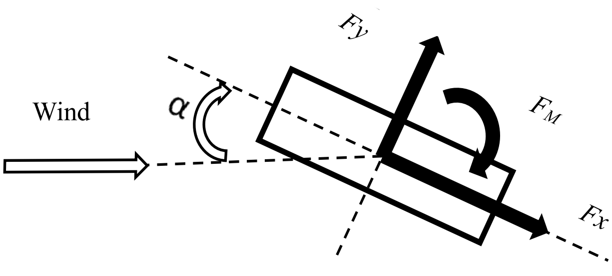

Fig. 6 Definitions of aerodynamic forces

The Scruton numbers for the vertical and torsional directions are defined as follows, respectively

$$S_{c\eta} = \frac{2m\delta_\eta}{\rho D^2} \tag{8}$$

Table 1 Characteristic parameters for the model (side ratio *B/D* = 3.24) used in free vibration experiments; the model has one vertical degree of freedom (1DOF) and the experiment is in smooth flow

Case name	Angle of attack	m (kg/m)	f (Hz)	δ_η	Sc_η
Closed girder	–3°	2.40	4.56	0.0028	4.5
	0°	2.40	4.57	0.0027	4.4
	+3°	2.40	4.55	0.0026	4.2
Open girder	–3°	2.36	4.60	0.0028	4.5
	0°	2.36	4.52	0.0029	4.5
	+3°	2.36	4.60	0.0029	4.5

Table 2 Characteristic parameters for the model (*B/D* = 5) used in free vibration experiments (torsional 1DOF, smooth flow)

Case name	Angle of attack	I (kg·m)	f (Hz)	δ_φ	Sc_φ
Closed girder	–3°	4.64×10^-2	6.41	0.0069	43
	0°	4.65×10^-2	6.41	0.0056	35
	+3°	4.63×10^-2	6.41	0.0063	39
Open girder	–3°	4.63×10^-2	6.45	0.0068	42
	0°	4.64×10^-2	6.42	0.0057	36
	+3°	4.56×10^-2	6.45	0.0073	45

Table 3 Characteristic parameters for the model (*B/D* = 5) used in free vibration experiments (vertical 1DOF, smooth flow)

Case name	Angle of attack	m (kg/m)	f (Hz)	δ_η	Sc_η
Closed girder	–3°	6.48	2.23	0.0027	8.5
	0°	6.49	2.23	0.0028	8.6
	+3°	6.47	2.23	0.0027	8.5
Open girder	–3°	6.40	2.25	0.0027	8.4
	0°	6.40	2.25	0.0027	8.4
	+3°	6.40	2.25	0.0027	8.4

$$S_{c\varphi} = \frac{2I\delta_\varphi}{\rho D^4} \tag{9}$$

where m is the mass per unit (kg/m), I is the moment of inertia per unit (kg·m), δ_η and δ_φ are the vertical and torsional structural damping quantified by logarithmic decrement, respectively, and ρ is the air density (kg/m^3).

The reduced wind velocity, Ur, is defined as follows

$$U_r = \frac{U}{fD} \tag{10}$$

2.4 Forced vibration tests

The aerodynamic self-excited forces due to wind encountering a girder can be calculated using the aerodynamic derivatives, as follows (Scanlan and Tomko 1971)

$$L_{\text{se}} = \frac{1}{2}\rho(2b)U^2\left\{kH_1^*\frac{\dot{\eta}}{U} + kH_2^*\frac{b\dot{\varphi}}{U} + k^2H_3^*\varphi + k^2H_4^*\frac{\eta}{b}\right\} \tag{11}$$

$$M_{\text{se}} = \frac{1}{2}\rho(2b^2)U^2\left\{kA_1^*\frac{\dot{\eta}}{U} + kA_2^*\frac{b\dot{\varphi}}{U} + k^2A_3^*\varphi + k^2A_4^*\frac{\eta}{b}\right\} \tag{12}$$

where L_{se} is the lift force per unit span (N/m), M_{se} is the pitching moment per unit span (N·m/m), η is the vertical displacement (m), φ is the torsional displacement (°), (·) indicates the time differentiation, b is the half-length of the width of the girder (m), k is the reduced frequency ($b\omega/U$), and ω is the angular frequency (rad/s).

Aerodynamic derivatives are used in practice to analyze galloping, torsional flutter, and coupled flutter. The coupled flutter, where the contribution of the coupling effect between torsional and vertical vibration is dominant, is mainly characterized by A_2^*, A_1^*, and H_3^* (Matsumoto 1996, Chen and Kareem 2006, Yang *et al*., 2007, Ge *et al*. 2016). Galloping is mainly characterized by positive H_1^*, whereas the torsional flutter is mainly characterized by positive A_2^* (Scanlan and Tomko 1971, Matsumoto 1996). Rather than the coupled flutter, the two models may show the galloping and torsional flutter. The effects of side openings on the galloping and torsional flutter were discussed based on the aerodynamic damping in vertical direction H_1^* and the aerodynamic damping in torsional direction A_2^*, which were identified from the vertical/torsional 1DOF forced vibration tests, respectively. Aerodynamic self-excited forces were measured by load cells rigidly connected to the model under vertical or torsional 1DOF forced vibration; the displacement of the model was simultaneously recorded using laser gages. The aerodynamic derivatives were then calculated based on the displacement and aerodynamic self-excited force time series.

Therefore, the vertical and torsional 1DOF forced vibration tests were conducted for the *B/D* = 3.24 model at α = 0° and +3°, and the torsional 1DOF vibration tests were conducted for the *B/D* = 5 model at α = 0° and +3°. To improve the accuracy of the flutter derivatives, the amplitude of the forced vibration cannot be too small to obtain large aerodynamic self-excited forces. Therefore, the vertical amplitude and frequency were set to 10 mm and 2 Hz, respectively, and the torsional amplitude and frequency were set to 2° and 2.6 Hz, respectively. The inertial forces were minimized as possible by setting a small mass and moment of inertia, and the inertial forces caused by the forced vibration were removed from the forces measured by the load cell.

2.5 Wind velocity measurement around the girder

The wind velocity distributions in the wake of the *B/D* = 3.24 girders with and without side openings were measured using an ‘X’ hot-wire anemometer; the wind velocity within the butterfly web girder was also measured. The

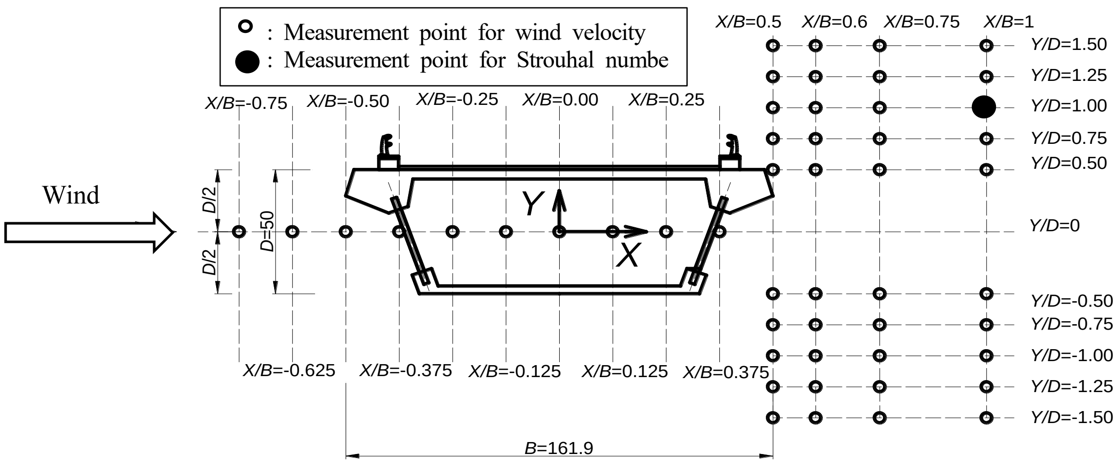

Fig. 7 Measurement points (*B/D* = 3.24 model) in the *X–Y* plane (unit: mm)

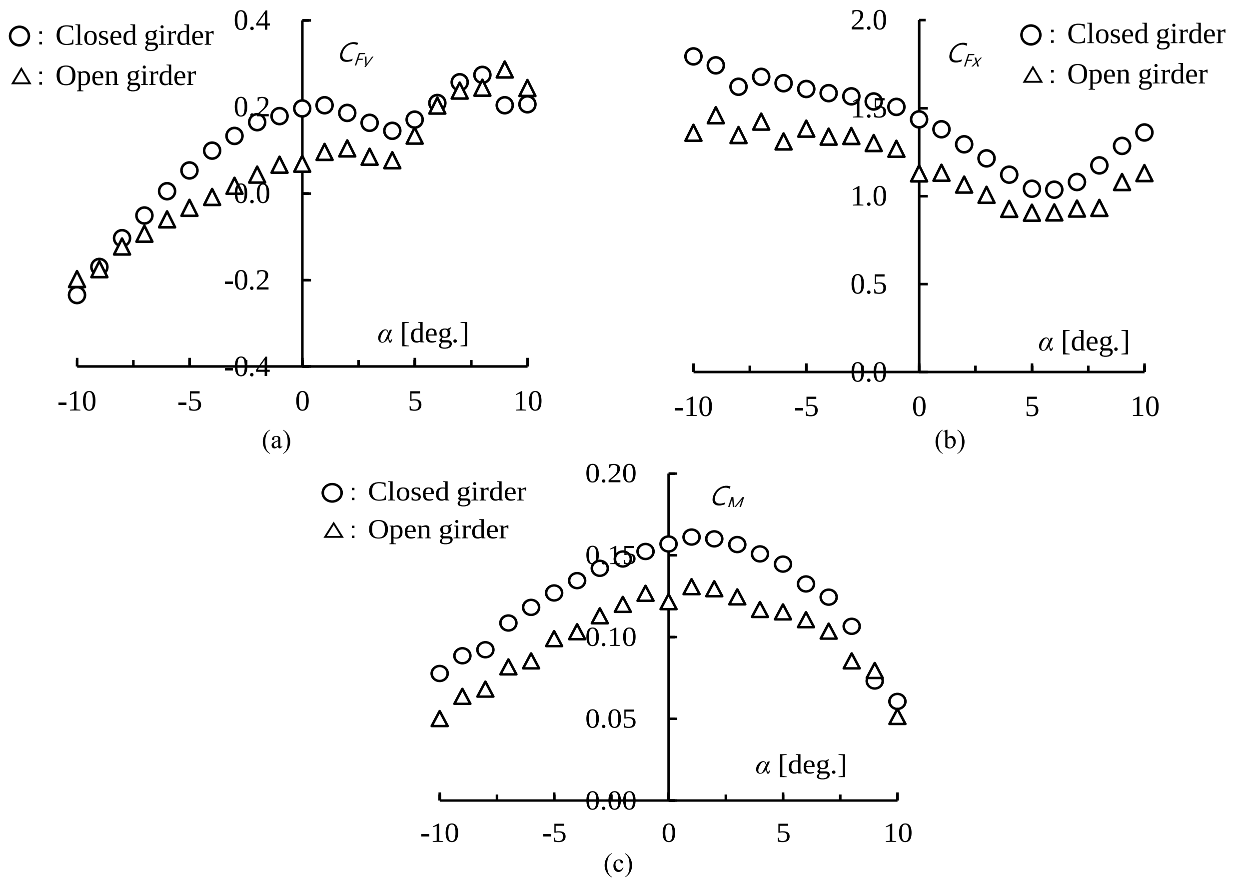

Fig. 8 Aerodynamic force coefficients (*B/D* = 3.24 model, *U* = 6 m/s, smooth flow) for (a) lift force C_{Fy}; (b) drag force C_{Fx}; (c) pitching moment C_M

measurement was performed with a sampling frequency of 1000Hz. An 'X' hot-wire anemometer provided the *X*- and *Y*-direction components of wind velocity. The measurement points and parameter definitions are shown in Fig. 7, where the origin of the coordinates is the center of the span and girder section, *X*/*B* and *Y/D* are non-dimensional coordinates in the main flow and vertical direction, respectively, and *Z* is the center distance in the span-wise \ direction. Because the center of the opening at the middle span coincides with the span center of the model (Fig. 4 (a)), the wind velocity distribution in the wake and inner space of the open girder was measured in the vertical plane (*X–Y* plane) at the span center (*Z* = 0). Meanwhile, the wind velocity distribution in the wake of the closed girder was also measured in the vertical plane (*X–Y* plane) at the span center (*Z* = 0). As a comparison with the frequency of vortex shedding identified from the fluctuating lift force, the frequency of vortex shedding was also calculated from the fluctuating wind velocity of the point of *X*/*B* = 1 and *Y*/*D* = 1.

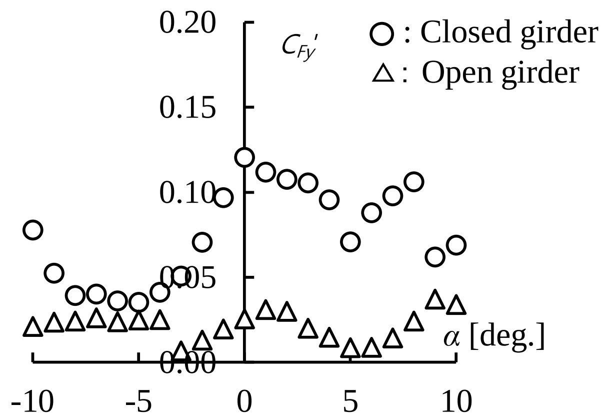

Fig. 9 Fluctuating lift force coefficient C_{Fy}' (B/D = 3.24 model, U = 6 m/s, smooth flow)

3. Aerodynamic performance of the B/D = 3.24 girder

3.1 Aerodynamic forces

The lift (C_{Fy}), drag (C_{Fx}), and pitching moment (C_M) coefficients are presented in the structural axis in Fig. 8(a) - (c), respectively. These coefficients showed the same trend in the closed and open girders. However, the absolute values of the coefficients of the open girder were smaller than those of the closed girder for each angle of attack. These results indicate that the side openings can reduce the lift, drag, and pitching moment. According to Fig. 8(a), the closed girder showed a negative gradient in the lift coefficient (C_{Fy}) at $1° \le \alpha \le 4°$, whereas the open girder had a negative slope at $2° \le \alpha \le 4°$. Because a negative gradient of the lift force indicates galloping instability, both the closed and open girders might show galloping instability at α = +3°. This is because with the change of α from 0° to +3°, the equivalent side ratio B'/D' decreased from 3.24 to 2.6. Meanwhile, the flow pattern around the girder changed from a reattachment type to a detachment type, which makes the model prone to galloping instability at α = +3°. Therefore, the discussion on the side opening effects focuses mainly on the results of the free vibration and forced vibration tests at α = +3°.

The Kármán vortex generates a large drag force coefficient and increases the curvature of a substantially separated flow (Bearman and Trueman 1972, Knisely *et al.* 2002, Matsumoto *et al.* 2006). Consequently, the smaller drag force coefficient of the open girder indicates the suppression of Kármán vortex shedding. As presented in Table 4, the Strouhal number identified from the fluctuating wind velocity (St = 0.171 for the closed girder; St = 0.174 for the open girder) and that from the fluctuating lift force (St = 0.167 for the closed girder; St = 0.164 for the open girder) were almost the same, indicating that the lift force fluctuates in the frequency of Kármán vortex shedding. Meanwhile, the fluctuating lift force coefficients of the open girder were smaller than those of the closed girder (Fig. 9), confirming that Kármán vortex shedding was suppressed owing to the side openings.

Table 4 Strouhal number identified from fluctuating lift force and fluctuating wind velocity (B/D = 3.24 model, U = 6 m/s, smooth flow, α = 0°)

	St of Closed girder	St of Open girder
Fluctuating lift force	0.167	0.164
Fluctuating wind velocity	0.171	0.174

3.2 Vertical 1DOF aerodynamic performance

The vertical aerodynamic responses of the closed and open girders at α = +3° are shown in Fig. 10. For convenient comparison of the free vibration and forced vibration test results, the double magnitude of the forced vibration is also included in the figure. U is the horizontal velocity of wind approaching the wind tunnel. The Scruton number was set to a small value for easier observation of the aerodynamic response (see Table 1). The symbol of two points connected by the vertical line indicates “limit cycle oscillation”. For the closed girder, vortex-induced vibration with the largest reduced double amplitude (0.42) occurred at a reduced wind velocity range ($4 < Ur < 6$) and galloping occurred at $Ur > 47$ (Fig. 10). The maximum reduced double amplitude of the vortex-induced vibration was 0.24, and galloping did not occur at $Ur < 70$ for the open girder (Fig. 10). Regarding vortex-induced vibration, the $1/St$ values for the closed and open girders were 5.78 (St = 0.173) and 5.99 (St = 0.167), respectively, which are slightly larger than $1.67B/D$ (= 5.41). Thus, the reduced critical wind velocity of the Kármán vortex vibration ($1/St$) was slightly larger than that of the motion-induced vortex vibration. Therefore, it is concluded that the vortex-induced vibration of the B/D = 3.24 model was of the motion-induced type. To discuss the effects of side openings on the critical wind velocity of galloping and aerodynamic damping further, the aerodynamic derivative H_1^* values of the closed and open girders at α = +3° are shown in Fig. 11. The reduced critical wind velocity of galloping was approximately Ur = 60 for the closed girder and approximately Ur = 80 for the open girder. These results demonstrate that galloping occurred in the open girder within the higher wind velocity range. The double magnitude of the vertical response of the closed girder reached 20 mm (the double amplitude of the forced vibration) at approximately Ur = 60 (Fig. 10), which was close to the reduced critical wind velocity of galloping (Ur = 60) observed in Fig. 11. Therefore, the critical wind velocity of galloping determined from the free vibration tests corresponded very well to that from the forced vibration tests, considering the aerodynamic damping corresponding to a double amplitude of 20 mm.

The H_1^* values for the closed girder obtained from the forced vibration test results were larger than those for the open girder in the high wind velocity range. These results indicate that the open girder was more stable than the closed girder at high wind velocities.

Therefore, the side openings can mitigate the motion-induced vortex vibration and stabilize the galloping. However, despite the suppression of Kármán vortex

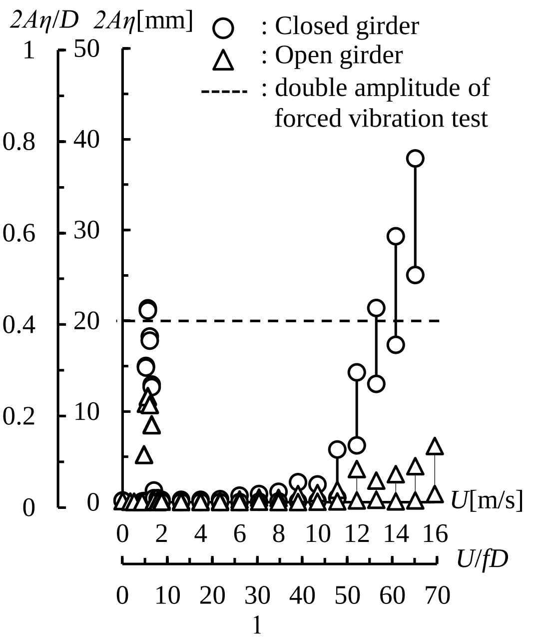

Fig. 10 Aerodynamic response of the *B/D* = 3.24 model (*B'/D'* = 2.6, vertical one degree of freedom (1DOF), α = +3°, smooth flow)

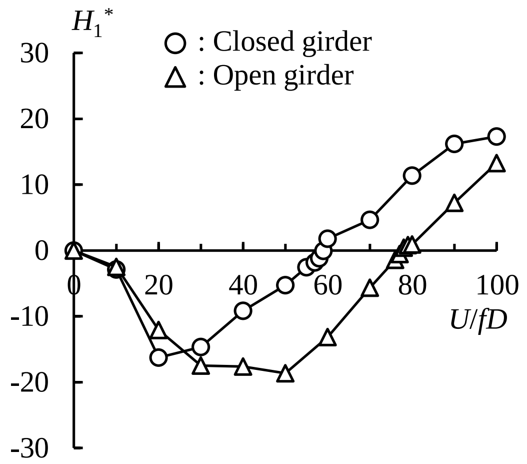

Fig. 11 Aerodynamic derivative H_1^* of the *B/D* = 3.24 model (*B'/D'* = 2.6, vertical 1DOF, α = +3°, f = 2.0 Hz, $2A\eta$ = 20 mm, smooth flow)

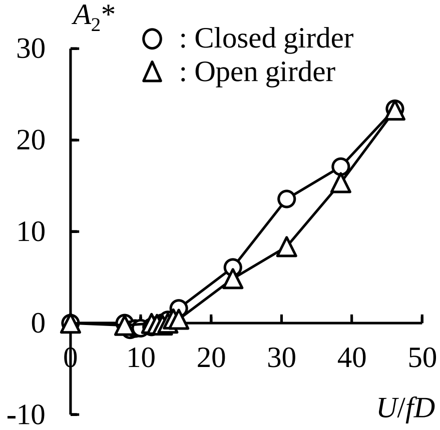

Fig. 12 Aerodynamic derivative A_2^* of the *B/D* = 3.24 model (*B'/D'* = 2.6, torsional 1DOF, α = +3°, f = 2.6 Hz, $2A\varphi$ = 4°, smooth flow)

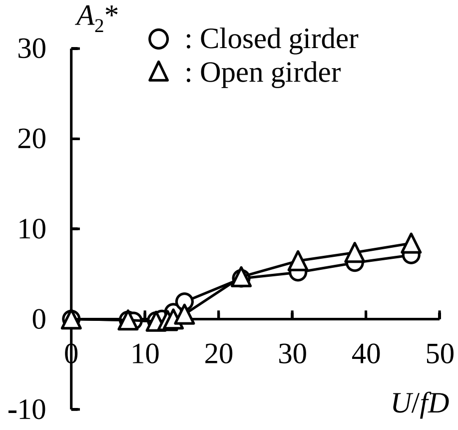

Fig. 13 Aerodynamic derivative A_2^* of the *B/D* = 3.24 model (*B'/D'* = 3.24, torsional 1DOF, α = 0°, f = 2.6 Hz, $2A\varphi$ = 4°, smooth flow)

shedding, demonstrated by the fluctuating lift force coefficient, the open girder still showed better galloping stability than the closed girder. To further discuss the effects of side openings, the flow field around and within the bridge deck will be investigated in the next section.

3.3 Torsional 1DOF aerodynamic performance

The same mechanism is responsible for motion-induced vortex vibration in both the vertical and torsional directions. Thus, for the torsional direction, only the effects of side openings on flutter instability are discussed, based on the forced vibration result. Figs. 12 and 13 show A_2^* of the closed and open girder at α = +3° and 0°. With the change in α from +3° to 0°, A_2^* was shown in the order that the equivalent side ratio *B'/D'* increases from 2.6 to 3.24. According to Fig. 12, at α = +3°, A_2^* of the closed girder has a positive value at Ur > 12, whereas that of the open girder is positive at Ur > 14. The A_2^* value of the closed girder is almost the same as that of the open girder. According to Fig. 13, at α = 0°, A_2^* of the closed girder also showed almost the same value as that of the open girder. By comparing Figs. 12 and 13, with the change in α from +3° to 0°, A_2^* of the closed/open girder obviously decreased. The decrease in A_2^* is related to the increase in the equivalent side ratio *B'/D'* from 2.6 to 3.24. This will be discussed later by comparing these results with the results of the *B/D* = 5 model. In summary, the side openings do not

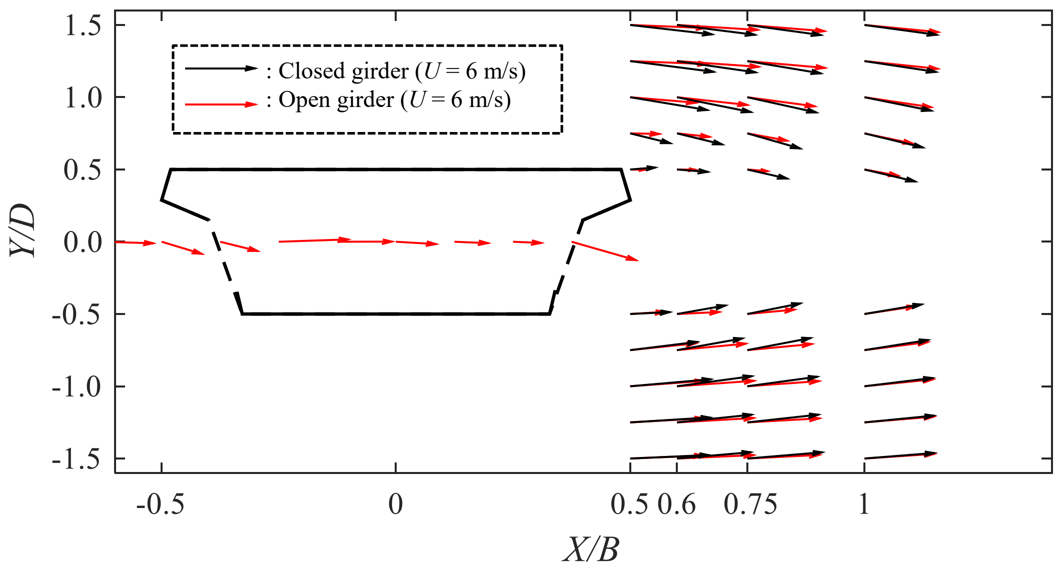

Fig. 14 Mean wind velocity vector distribution in the wake of the *B*/*D* = 3.24 model (*α* = 0°, *U* = 6 m/s, smooth flow). The black arrow represents the wind velocity vector of the closed girder. The red arrow represents the wind velocity vector of the open girder

have obvious effects on the critical wind velocity of the torsional flutter and aerodynamic damping in the torsional direction.

4. Flow field characteristics in the wake and inner space of the B/D = 3.24 girder

As discussed in the previous section, the side openings contributed to the suppression of Kármán vortex shedding. According to a previous study (Yagi *et al*. 2013), the mitigation of Kármán-vortex shedding can lead to galloping instability. However, side openings can still stabilize the galloping. To clarify the mechanism of the side opening effects on aerodynamic performance, wind velocity measurements in the wake and inner space of the *B*/*D* = 3.24 model were conducted.

Because the center of the opening coincides with the span center, for both the closed girder and open girder, the mean wind velocity distribution in the wake was measured in the vertical plane (*X*–*Y* plane) at the span center of the model (*Z* = 0) (Fig. 7). By comparing the mean wind velocity vectors in the wakes of the closed and open girders, the effects of side openings on the time-averaged streamline were examined.

Fig. 14 shows the distributions of mean wind velocity vectors in the wakes of the closed and open girders along the *Y*-direction at *X*/*B* = 0.50, 0.60, 0.75, and 1.00. The approaching wind velocity vector of 6 m/s is also included in the plot, which has the same scale as the mean wind velocity vectors in the wake. The mean wind velocity vectors in the wake of the closed girder were generally different in magnitude and/or direction from those of the open girder. More specifically, the vectors of the closed girder at $|Y/D| \geq 0.5$ and $0.5 \leq X/B \leq 1$ exhibited larger angles between the vector and the *X*-direction than those at the opening center of the open girder. This indicates that the side openings reduced the curvature of the time-averaged streamline in the wake.

The curvature of the time-averaged streamline in the wake was reduced by the side openings. The curvature of the time-averaged streamline in the wake of the rectangular cylinder was reduced by increasing the side ratio (Nakaguchi 1968). The side openings likely reduced the curvature of the time-averaged streamline in a similar way to the reduction in curvature due to the increase in side ratio. Meanwhile, by increasing the side ratio, it enhances the reattachment of the time-averaged flow field on the side surface (Nakaguchi 1968). Therefore, the small curvature of the time-averaged streamline in the wake due to the side openings indicates that they equivalently increase the side ratio and enhance the reattachment of the separated shear layer on the model side surface. Owing to the reattachment of the time-averaged shear layer on the surface, the critical wind velocity of the galloping can be increased (Bearman and Tureman 1972, Mizota and Okajima 1981, Kwok and Melbourne 1977, Nakamura *et al*. 1991). Consequently, by enhancing the reattachment of the separated shear layer on the side surface for the *B*/*D* = 3.24 model at *α* = +3°, the side opening stabilized the galloping.

As shown in Fig. 14, at high wind velocities, the flow reaches the inner space of the girder and bursts out from the downstream-side opening. Because the flow from the downstream opening can disturb the fluid entrainment in the wake and the formation of the reversed flow (Bearman and Trueman 1972, Laneville and Yong 1983, Deniz and Staubli 1997), the smaller curvature of the time-averaged streamline around an open girder may be related to the outflow from downstream openings.

With internal distance, the side openings are discretely distributed along the span-wise direction. Therefore, the outflow from the side openings may cause the flow field

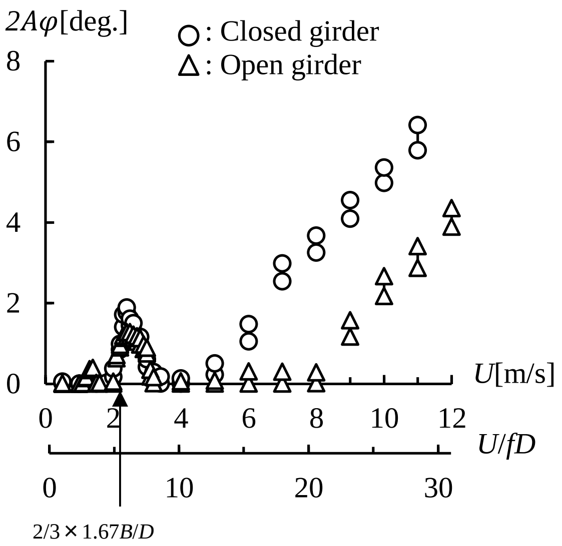

Fig. 15 Aerodynamic response of the B/D = 5 model (B'/D' = 4.1, torsional 1DOF, α = +3°, smooth flow)

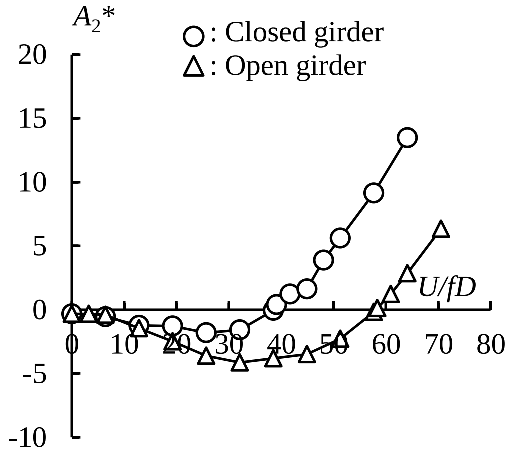

Fig. 16 Aerodynamic derivative A_2^* of the B/D = 5 model (B'/D' = 4.1, torsional 1DOF, α = +3°, f =2.6 Hz, $2A\varphi$ = 4°, smooth flow)

around the girder to change along the span-wise direction, exhibiting three-dimensional characteristics. This is consistent with the low correlation of the fluctuating wind velocity in the wake of a stationary and oscillating square cylinder with side openings observed in the previous studies (Nakato 2016). Because the reduction in the correlation of wind velocity may lead to a decrease in the correlation of forces working on the model along the span, the three-dimensional effects of flow field may be another reason for the stabilization of vibration owing to the side openings.

In summary, potentially affected by the outflow from the side opening in the wake, the time-averaged flow field around the girder is changed owing to the side openings.

5. Aerodynamic performance of the B/D = 5 girder

As discussed previously, the galloping instability and motion-induced vortex vibration of the B/D = 3.24 model were stabilized by the side openings. However, the side openings exhibited no significant effects on torsional flutter instability in the B/D = 3.24 model. Therefore, the effects of side openings on the aerodynamic performance of the slenderer girder (B/D = 5) are discussed in this section. The aerodynamic force of the stationary B/D = 5 model was not observed to fluctuate in a frequency of vortex shedding owing to the flow field of the reattachment type. Because of the flow pattern of the reattachment type, the B/D = 5 model should experience torsional flutter instability rather than galloping instability. Therefore, vertical 1DOF and torsional 1DOF free vibration tests, and torsional 1DOF forced vibration tests are conducted for the B/D = 5 model. The results of the torsional 1DOF free vibration tests and forced vibration tests are shown in the order that the equivalent side ratio of the B/D = 5 model increased from B'/D' = 4.1 to B'/D' = 5 with the change of α from +3° to 0°.

A previous study (Matsumoto *et al*. 2006) demonstrated that the reduced critical wind velocity of the Kármán vortex vibration ($1/St$) was slightly larger than that of the motion-induced vortex vibration (vertical direction 1.67B/D and torsional direction 2/3 × 1.67B/D) for a B/D = 5 rectangular cylinder. In such a case, the vortex-induced vibration is mainly of the motion-induced type. The vortex-induced vibration of the B/D = 5 model, which is a rectangular cylinder-like structure, is therefore of the motion-induced type.

5.1 Torsional 1DOF aerodynamic performance

The results of the torsional 1DOF free and forced vibration tests at α = +3° are shown in Figs. 15 and 16, respectively. The B/D = 5 model at α = +3° has an equivalent side ratio of B'/D' = 4.1. The horizontal axis U in Fig. 15 is the approaching wind velocity in the wind tunnel. The Scruton number was set to a small value for the 1DOF torsional free vibration system (Table 2). The symbol of two points connected by the vertical line indicates "limit cycle oscillation". As shown in Fig. 15, the vortex-induced vibration for both the closed and open girder occurred at approximately Ur = 5, which is close to 2/3×1.67B/D (Eq. (2)), confirming that the vortex-induced vibration is of the motion-induced type. The largest double amplitude of the torsional motion-induced vortex vibration for the closed girder was 2.1°, and that of the open girder was 1.7°. The reduced critical wind velocity of torsional flutter was 10 for the closed girder and 20 for the open girder. According to Fig. 16, based on A_2^*, torsional flutter instability was evident in the closed girder at Ur > 40 and in the open girder at Ur > 60. However, according to Fig. 15, the double amplitude of the vibration reached 4° at Ur = 23 in the closed girder, which was the double amplitude of the forced vibration, and this value (Ur = 23) was far smaller than that

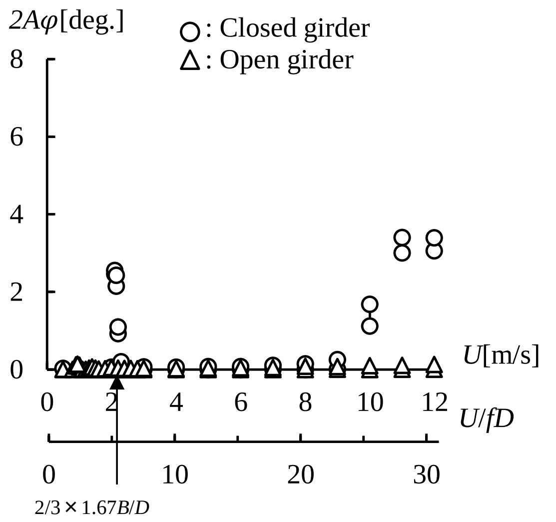

Fig. 17 Aerodynamic response of the *B/D* = 5 model (*B'/D'* = 5, torsional 1DOF, α = 0°, smooth flow)

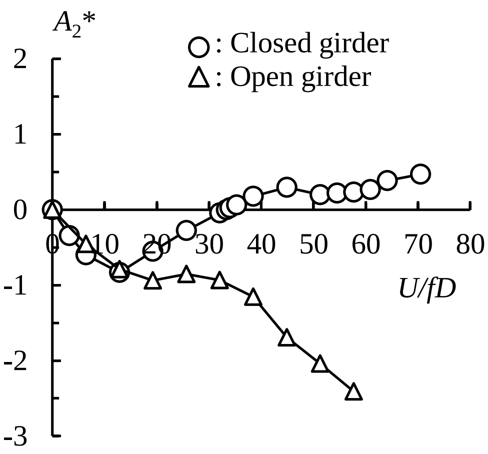

Fig. 18 Aerodynamic derivative A_2^* of the *B/D* = 5 model (*B'/D'* = 5, torsional 1DOF, α = 0°, *f* =2.6 Hz, $2A\varphi$ = 4°, smooth flow)

(*Ur* = 40) of the forced vibration (Fig. 16). In the open girder, the cross point of the double amplitude of the vibration and 4° occurred at *Ur* = 32 (Fig. 15), which was far smaller than that (*Ur* = 60) observed in the forced vibration test (Fig. 16). This result indicates that at α = +3°, the results of the free vibration and forced vibration tests did not correspond well. However, the results of these tests still demonstrate qualitatively that the side openings can stabilize the motion-induced vortex vibration and torsional flutter

The torsional vibration responses and aerodynamic derivative A_2^* of the closed and open girders at α = 0° are shown in Figs. 17 and 18. The *B/D* = 5 model at α = 0° has an equivalent side ratio of *B'*/*D'* = 5. According to Fig. 17, the vortex-induced vibration for both the closed and open girder occurred at approximately *Ur* = 5, which is close to 2/3 × 1.67*B/D* (Eq. (2)). This also confirmed that the vortex-induced vibration is of the motion-induced type. The double amplitude of the torsional motion-induced vortex vibration for the closed girder at α = 0° was 2.4°, and that for the open girder was almost 0° (Fig. 17). These results confirmed that the side openings diminished the torsional motion-induced vortex vibration. Additionally, the closed girder exhibited torsional flutter instability at *Ur* > 23 and the open girder did not show torsional flutter instability until *Ur* = 32. Thus, the torsional flutter was mitigated by the side openings. This finding was further confirmed by the aerodynamic derivative A_2^* (Fig. 18), whose positive value indicates aerodynamic instability. The closed girder showed torsional flutter instability at *Ur* > 32 and the open girder did not show torsional flutter until *Ur* = 60 (Fig. 18). Moreover, as shown in Fig. 17, the double amplitude of torsional vibration of the closed girder was less than 4° until *Ur* = 32, which is the double amplitude of the forced vibration. Because the double amplitude of the aerodynamic response at *Ur* = 32 was close to 4° (Fig. 17), the critical wind velocity of torsional flutter in the free vibration test was close to that of forced vibration (*Ur* = 32) considering the aerodynamic damping corresponding to a double amplitude of 4° (Fig. 18). Therefore, the reduced critical wind velocity of torsional flutter in the free vibration test corresponds well with that of the forced vibration test.

Comparing Figs. 12, 13, 16, and 18 shows that the side openings had no effects on the torsional flutter for the *B*/*D* = 3.24 model at α = +3° and 0°, but increased the reduced critical wind velocity of the torsional flutter from *Ur* = 60 to *Ur* = 80 for the *B*/*D* = 5 model at α = +3°, and totally mitigated the torsional flutter for the *B*/*D* = 5 model at α = 0°. In terms of this difference in the effects of the side openings on torsional flutter between these two models, the model configuration may play an important role. As mentioned before, the opening area ratio is 15.5% for the *B*/*D* = 3.24 model and 16.7% for the *B*/*D* = 5 model. Therefore, rather than the opening area ratio, the equivalent side ratio *B'*/*D'* of the model probably plays the main role. By comparing Figs. 12, 13, 16, and 18, the torsional flutter of the model with equivalent side ratio *B'*/*D'* = 2.6 and 3.24 was characterized by the relatively large A_2^*, while the torsional flutter of the model with equivalent side ratio *B'*/*D'* = 4.1 and 5 was characterized by the relatively small A_2^*. Therefore, A_2^* of the closed girder gradually decreased with the increase in equivalent side ratio from *B'*/*D'* = 2.6 to *B'*/*D'* = 5. Meanwhile, as shown in Fig. 19, A_2^* decreased with the increase in side ratio from 3 to 10 for the rectangular cylinder. Similar to the decrease in A_2^* with the increase in side ratio for the rectangular cylinder, A_2^* of these two models decreased owing to the increase in equivalent side ratio *B'*/*D'*. Furthermore, the torsional flutter of the rectangular cylinder gradually switches from the wind velocity-restricted type to the divergent type with an increase in side ratio from 2 to 10, because the flow pattern gradually changes from the intermittent reattachment type to the steady reattachment type (Matsumoto *et al*. 1997). Possibly because of the change in flow pattern with the side ratio, the side openings did not have effects on the torsional flutter characterized by the comparatively large A_2^*, but stabilized that characterized by the comparatively small A_2^*.

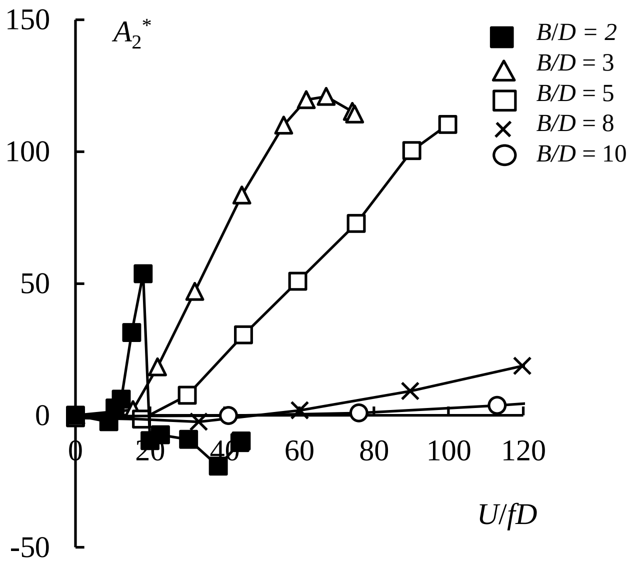

Fig. 19 A_2^* of the rectangular cylinder with different side ratios (Matsumoto 1996)

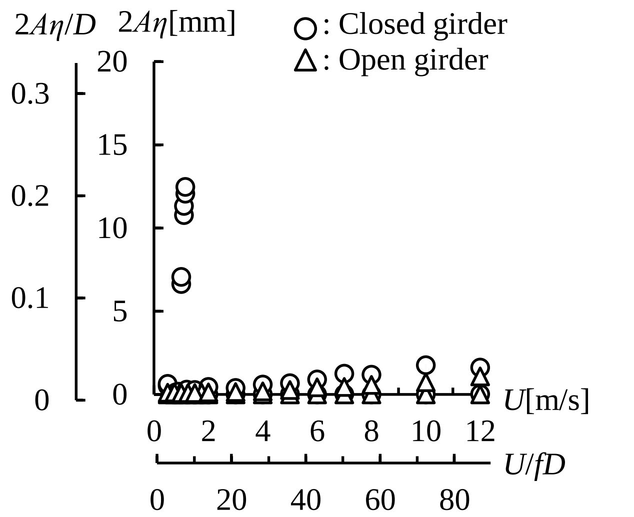

Fig. 20 Aerodynamic response of the B/D = 5 model (B'/D' = 5, vertical 1DOF, α = 0°, smooth flow)

5.2 Vertical 1DOF aerodynamic performance

The vertical 1DOF aerodynamic performances of the closed and open girders at α = 0° are summarized in Fig. 20. The mass and damping of the system were minimized as much as possible to more clearly observe the responses of the closed and open girders (Table 3). The largest reduced double amplitude of the motion-induced vortex vibration of the closed girder was approximately 0.23, whereas that of the open girder was almost 0. Consequently, the side openings mitigated the motion-induced vortex vibration for the B/D = 5 model. Neither the closed nor the open girder exhibited galloping instability. However, the closed girder showed larger amplitude than the open girder at high wind velocities, indicating that side openings can limit the amplitude of the vertical vibration at high wind velocities.

6. Conclusions

To investigate the effects of side openings on the aerodynamic performance of box girders, two butterfly web girders with side ratios of 3.24 and 5 were used in this research. A series of wind tunnel tests, that is, aerodynamic force tests, free vibration tests, and forced vibration tests, were carried out for these two butterfly web girders. To further investigate the effects of side openings on the flow field, the wind velocity in the wake of a butterfly web girder with a side ratio of 3.24 was also measured. The conclusions are summarized as follows:

- The side openings suppressed the Kármán vortex shedding. Meanwhile, the side openings stabilized the motion-induced vortex vibration in both the vertical and torsional directions.
- The side openings increased the critical wind velocity of galloping. This may be because the side openings enhanced the reattachment of the time-averaged flow on the girder side surface.
- The side openings had no significant effects on the torsional flutter for the model with a side ratio of 3.24, while they stabilized the torsional flutter for the model with a side ratio of 5. This is probably because the mechanism of torsional flutter changed with the increase in side ratio.

The two girders proved to have good aerodynamic performance owing to the discretely distributed side openings. The use of side openings is a promising method to design strong and light box girders with good aerodynamic performance.

Acknowledgements

The authors gratefully acknowledge the valuable contribution of the late Professor Hiromichi Shirato in this research.

References

Andrianne, T. and Dimitriadis, G. (2013), "Experimental and numerical investigations of the torsional flutter oscillations of a 4:1 rectangular cylinder", *J. Fluids Struct.*, **41**, 64-88.

Bearman, P. and Trueman, D. (1972), "An investigation of the flow around rectangular cylinders", *Aeronautical Quarterly*, **23**(3), 229-237. https://doi.org/10.1017/S0001925900006119.

Billah, K.Y. and Scanlan, R.H. (1991), "Resonance, Tacoma Narrows bridge failure, and undergraduate physics textbooks", *Am. J. Phys.*, **59**, 118-124. https://doi.org/10.1119/1.16590.

Chen, X. and Kareem, A. (2006), "Revisiting Multimode Coupled Bridge Flutter: Some New Insights", *J. Eng. Mech.*, **132**, 1115-1123.https://doi.org/10.1061/(ASCE)0733-9399(2006)132:10(1115).

Den Hartog and J.P. (1985), *Mechanical Vibrations*, Dover Publication, New York, NY, USA.

Deniz, S. and Staubli, T. (1997), "Oscillating rectangular and octagonal profiles: Interaction of leading- and trailing-edge vortex formation", *J. Fluids Struct.*, **11**, 3-31. https://doi.org/10.1006/jfls.1996.0065.

Dong, H., Cao, S. and Ge, Y. (2017), "Large-eddy simulation of stably stratified flow past a rectangular cylinder in a channel of finite depth", *J. Wind Eng. Ind. Aerod.*, **170**, 214-225.

https://doi.org/10.1016/j.jweia.2017.08.019.

Ge, Y., Liu, Z. and Yang, Y. (2016), "Energy conversion mechanism of aerodynamic flutter of a box girder", *Proceedings of the First International Symposium on Flutter and its Application*, Tokyo, Japan, May. https://repository.exst.jaxa.jp/dspace/handle/a-is/612470

Hu, G., Tse, K.T. and Kwok, K.C.S. (2016), "Aerodynamic mechanisms of galloping of an inclined square cylinder", *J. Wind Eng. Ind. Aerod.*, **148**, 6-17. https://doi.org/10.1016/j.jweia.2015.10.011.

Hourigan, K., Thompson, M. C. and Tan, B. T. (2001), "Self-sustained oscillations in flows around long blunt plates", *J. Fluids Struct.*, **15**, 387-398. https://doi.org/10.1006/jfls.2000.0352.

Kasuga, A. (2015), "Multi-span extradosed bridge", *Proceeding of International Conference on Multi-span Large Bridges*, Porto, Portugal, July.

Kasuga, A. (2017), "Effects of butterfly web design on bridge construction", *Struct. Concr.*, **18**(a), 128-142. https://doi.org/10.1002/suco.201600109.

Komatsu, S. and Kobayashi, H. (1980), "Vortex-induced oscillation of bluff cylinders", *J. Wind Eng. Ind. Aerod*., **6**, 335-362. https://doi.org/10.1016/0167-6105(80)90010-0.

Kwok, K.C.S. and Melbourne, W.H. (1977), "The effects of freestream turbulence on a galloping square tower", *Proceedings of the 6th Australasian Hydraulics and Fluid Mechanics Conference*, Adelaide, Australia, December.

Knisely, B.C., Matsumoto, M. and Menacher, F. (1987), "Rectangular cylinders in flows with harmonic perturbations", *J. Hydraul. Eng.*, **112**, 690-704. https://doi.org/10.1061/(ASCE)0733-9429(1986)112:8(690).

Kumar, R.A., Sohn, C.H. and Gowda, B.H.L. (2009), "Influence of corner radius on the near wake structure of a transversely oscillating square cylinder", *J. Mech. Sci. Technol.*, **23**, 2390-2416. https://doi.org/10.1007/s12206-009-0630-y.

Laneville, A. and Yong L.Y. (1983), "Mean flow patterns around two-dimensional rectangular cylinders and their interpretation", *J. Wind Eng. Ind. Aerod*., **14**, 387-398. https://doi.org/10.1016/0167-6105(83)90040-5.

Li, M., Li, S., Liao, H., Zeng, J. and Wang, Q. (2016), "Spanwise correlation of aerodynamic forces on oscillating rectangular cylinder", *J. Wind Eng. Ind. Aerod.*, **154**, 47-57. https://doi.org/10.1016/j.jweia.2016.04.003.

Matsumoto, M., Daito, Y., Yoshizumi, F., Ichikawa, Y. and Yabutani, T. (1997), "Torsional flutter of bluff bodies", *J. Wind Eng. Ind. Aerod*., **69**-**71**, 871-882. https://doi.org/10.1016/S0167-6105(97)00213-4.

Matsumoto, M. (1996), "Aerodynamic damping of prisms", *J. Wind Eng. Ind. Aerod.*, **59**, 159-175. https://doi.org/10.1016/0167-6105(96)00005-0.

Matsumoto, M., Yagi T., Lee, J.H., Hori, K. and Kawashima, Y. (2006), "Karman vortex effect on the aerodynamic forces to rectangular cylinders", *ASME Pressure Vessels and Piping/ICPVT-11 Conference*, Vancouver, BC, Canada, July.

Matsumoto, M., Yagi, T., Tamaki, H. and Tsubota, T. (2008a), "Vortex-induced vibration and its effect on torsional flutter instability in the case of B/D = 4 rectangular cylinder", *J. Wind Eng. Ind. Aerod.*, **96**(6-7), 971-983. https://doi.org/10.1016/j.jweia.2007.06.023.

Matsumoto, M., Hashimoto, M., Yagi, T., Nakase, T. and Maeta, K. (2008b), "Steady galloping/unsteady galloping and vortex-induced vibration of bluff bodies associated with mitigation of Kármán vortex", *Proceeding of 6th International Colloquium on Bluff Body Aerodynamics and Applications*, Milan, Italy, July.

Mills, R., Sheridan, J. and Hourigan, K. (2003), "Particle image velocimetry and visualization of natural and forced flow around rectangular cylinders", *J. Fluid Mech.*, **478**, 299-323. https://doi.org/10.1017/S0022112002003439.

Mizota, T. and Okajima, A. (1981), "Experimental studies of time mean flows around rectangular prisms", *Proc. Japan Soc. Civ. Eng.*, **312**, 39-47. (in Japanese).

Nakaguchi, H., Hashimoto, K. and Muto, S. (1968), "An experimental study on aerodynamic drag of rectangular cylinders", *Trans. Japan. Soc. Aero. Space. Sci.*, **16**, 1-5. (in Japanese).

Nakamura, Y. and Nakashima, M. (1986), "Vortex excitation of prisms with elongated rectangular, H and [vdash] cross-sections", *J. Fluids Struct.*, **163**, 149-169. https://doi.org/10.1017/S0022112086002252.

Nakamura, Y. and Hirata, K. (1994), "The aerodynamic mechanism of galloping", *Trans. Jpn. Soc. Aeronaut. Space Sci.*, **36**, 257-269.

Nakamura, Y., Hirata, K. and Urabe, T. (1991), "Galloping of rectangular cylinders in the presence of a splitter plate", *J. Fluids Struct.*, **5**(5), 521-549. https://doi.org/10.1016/S0889-9746(05)80004-0.

Nakato, S. (2016), "Correlation of fluctuating velocity in the wake of an oscillating square cylinder with openings or appendages", *Proceeding of First International Symposium on Flutter and its Application* (*ISFA2016*), Tokyo, Japan, May.

Naudascher, E., Weske, J.R. and Fey, B. (1981), "Exploratory study on damping of galloping vibrations", *J. Wind Eng. Ind. Aerod.*, **8**, 211-222. https://doi.org/10.1016/0167-6105(81)90020-9.

Naudascher, E. and Wang, Y. (1993), "Flow-induced vibrations of prismatic bodies and grids of prisms", *J. Fluids Struct.*, **7**, 341-373. https://doi.org/10.1006/jfls.1993.1021.

Nguyen, D.T., Hargreaves, D.M. and Owen, J.S. (2018), "Vortex-induced vibration of a 5:1 rectangular cylinder: A comparison of wind tunnel sectional model tests and computational simulations", *J. Wind Eng. Ind. Aerod*., **175**, 1-16. https://doi.org/10.1016/j.jweia.2018.01.029.

Okajima, A., Abe, A. and Kiwata, K. (1990), "Aeroelastic instability of two rectangular cylinders in a tandem arrangement", *J. Struct. Eng. A* (*JSCE*), **36**(b), 859-864 (in Japanese).

Parkinson, G. V. and Smith, J. D. (1964), "The square prisms as an aeroelastic non-linear oscillator", *Quarterly J. Mech. Appl. Math.*, **17**, 225-239. https://doi.org/10.1093/qjmam/17.2.225.

Parkinson, G. V. and Sullivan, P.P. (1979), "Galloping response of towers", *J. Wind Eng. Ind. Aerod.*, **4**, 253-260. https://doi.org/10.1016/0167-6105(79)90006-0.

Scanlan, R. H. and Tomko, J. (1971), "Air foil and bridge deck flutter derivatives", *J. Eng. Mech*., **97**(6), 1717-1937.

Shiraishi, N. and Matsumoto, M. (1983), "On classification of vortex-induced oscillation and its application for bridge structures", *J. Wind Eng. Ind. Aerod*., **14**(1-3), 419-430. https://doi.org/10.1016/0167-6105(83)90043-0.

Wu, T. and Kareem, A. (2012), "An overview of vortex-induced vibration (VIV) of bridge decks", *Front. Archit. Civ. Eng.*, **6**, 335-347. https://doi.org/10.1007/s11709-012-0179-1.

Yagi, T., Shinjo, K., Narita, S., Nakase, T. and Shirato, H. (2013), "Interferences of vortex sheddings in galloping instability of rectangular cylinders", *J. Struct. Eng. A* (*JSCE*), **59**A, 552-561 (in Japanese).

Yang, Y., Ge, Y. and Xiang, H. (2007), "Investigation on flutter mechanism of long-span bridges with 2d-3DOF method", *Wind Struct.*, **10**(5), 421-435. https://doi.org/10.12989/was.2007.10.5.421.

CC